Liquefaction Evaluation of Interbedded Soil Deposit: Çark Canal in 1999 M7.5 Kocaeli Earthquake

By

Ross W. Boulanger, Ph.D., P.E., F.ASCE
Corresponding author: Professor, Department of Civil and Environmental Engineering, University of California, Davis, CA 95616, rwboulanger@ucdavis.edu

Sean K. Munter
Staff Engineer, GeoPentech, Irvine, CA 92617, sean_munter@geopentech.com

Christopher P. Krage, Ph.D., M.ASCE
Project Professional, GEI Consultants, Rancho Cordova, CA 95670, ckrage@geiconsultants.com

Jason T. DeJong, Ph.D., M.ASCE
Professor, Department of Civil and Environmental Engineering, University of California, Davis, CA 95616, jdejong@ucdavis.edu

Abstract

The performance of Çark Canal in the 1999 M=7.5 Kocaeli earthquake is evaluated using common liquefaction vulnerability index (LVI) methods, a nonlinear dynamic analysis (NDA) method, and a Newmark sliding block method to examine possible factors contributing to why different analysis approaches often overestimate liquefaction effects in interbedded deposits. The characterization of the interbedded fluvial stratum based on cone penetration test (CPT) data utilized an inverse filtering procedure to correct CPT data for thin layer and transition zone effects. Common LVIs computed using the measured and inverse filtered CPT data with a site-specific fines content calibration show that the combination of these two steps reduce the LVIs by 30-50% for this site and seismic loading. Two-dimensional NDAs are performed using stochastic realizations for the interbedded stratum and the PM4Sand and PM4Silt constitutive models for the sand-like and clay-like portions, respectively. Computed deformations are evaluated for their sensitivity to stochastic model parameters, the cyclic strength assigned to the sand-like soils, the undrained shear strengths assigned to the clay-like soils, the level of shaking, and other input parameters. Newmark sliding block analyses are performed with different allowances for how inter-bedding influences the composite strength of the interbedded stratum. The differences between results obtained with these analysis methods, along with those presented by Youd et al. (2009), provide insights on how the various factors can contribute to an over-estimation of ground deformations in interbedded deposits of sands, silts, and clays.

Introduction

Methods for predicting ground deformations due to earthquake-induced liquefaction include empirical regression models (e.g., Youd et al. 2002), Newmark sliding block models (e.g., Olson & Johnson 2008), various one-dimensional (1-D) liquefaction vulnerability indices (LVIs), and nonlinear dynamic response analyses (NDAs). One-dimensional LVIs are computed using data from individual borings or cone penetration test (CPT) soundings, and include the lateral displacement index (LDI), liquefaction potential index (LPI), liquefaction severity number (LSN), and post-liquefaction re-consolidation settlement (S_{v-1D}). Empirical regression models, Newmark sliding block models, and LVIs have significant limitations due to their simplifying assumptions, including not modeling any dynamics, but are relatively easy to perform and can be sufficient for reaching appropriate decisions for many situations. NDAs do not include as many simplifying assumptions and thus are applicable to a broader range of conditions; however, they require considerably more engineering expertise and effort to perform.

Case history studies have shown that LVIs and empirical regression models can tend to over-predict earthquake-induced liquefaction effects in interbedded deposits of sand, silt and clay. The tendency for LVIs computed using common practices to over-predict liquefaction effects at interbedded sites was observed after the 1999 M=7.5 Kocaeli earthquake (e.g., Youd et al. 2009), the 1999 M=7.6 Chi-Chi

earthquake (e.g., Chu et al. 2007), and the 2010-2011 Canterbury Earthquake Sequence (e.g., Beyzaei et al. 2018, Maurer et al. 2014, van Ballegooy et al. 2014).

Possible factors that can contribute to an over-estimation of liquefaction effects in interbedded deposits may be grouped into three categories (Boulanger et al. 2016): (1) limitations in site characterization tools and procedures, (2) limitations in the correlations used for evaluating liquefaction triggering and consequences, and (3) limitations from analysis approaches and neglected mechanisms. Limitations within each of these categories that are believed to have a significant role in different situations are summarized in Table 1. Limitations associated with site characterization include: thin layer and transition zone effects on penetration test results; differentiating between distinct interfaces (e.g., erosional contacts) and gradual transitions (e.g., graded bedding); quantifying the lateral continuity of weak or liquefiable layers; and accounting for partial saturation below a water table. Limitations in triggering and strain correlations stem from the paucity of data for intermediate soils with certain ranges of fines content (FC) and plasticity index (PI), plus the fact that factors such as age, stress and strain history, lateral earth pressure at rest (i.e., K_o), and cementation are not explicitly accounted for. Limitations in analysis methods can include: conservative assumptions of lateral continuity for the weak or liquefiable soils; neglecting the beneficial effect of a thick crust layer in reducing surface manifestations of liquefaction at depth in areas without lateral spreading; not accounting for how dynamic response and excess pore pressure diffusion processes affect the dynamic stresses and deformations in a soil profile; and not accounting for how the two- and three-dimensional (2D and 3D) geometry affects dynamic response and deformations. For most case histories with an over-prediction of liquefaction effects, it is likely that the over-prediction stems from the cumulative effect of several factors, with the impact of each factor depending on the specific site conditions, seismic loading, and analysis methods.

The performance of Çark Canal in the 1999 M=7.5 Kocaeli earthquake is an example of a site with interbedded fluvial deposits that did not develop significant visible damage despite an estimated peak ground acceleration (PGA) of about 0.4 g. Liquefaction evaluations using alternative susceptibility criteria and a multilinear regression model predicted relatively large ground deformations (0.7 to 2.6 m) due to liquefaction of silty sand layers, whereas a Newmark sliding block analysis that assumed the strength of the interbedded fluvial sediments was equal to that of the clay-like portions alone correctly predicted negligible displacements (Youd et al. 2009). That study concluded that the "absence of lateral spread… indicates that these [liquefiable] layers were most likely discontinuous lenses with sufficient shear resistance in the discontinuities to prevent lateral spread" (Youd et al. 2009).

The present study evaluates the performance of Çark Canal in the Kocaeli earthquake using LVI, NDA, and Newmark methods to examine possible factors contributing to why different approaches often overestimate liquefaction effects in interbedded deposits. First, the characterization of the interbedded

fluvial stratum based on cone penetration test (CPT) data is revisited using the inverse filtering procedure developed by Boulanger and DeJong (2018) to correct CPT data for thin layer and transition zone effects. Common LVIs are computed using the measured and inverse filtered CPT data with a site-specific FC calibration to show that the combination of these two steps reduced the LVIs by 30-50% for this site and seismic loading. Two-dimensional NDAs are performed using stochastic realizations for the interbedded stratum based on a transition probability approach. The sand-like and clay-like portions of the interbedded stratum are modeled using the PM4Sand (Boulanger and Ziotopoulou 2017) and PM4Silt (Boulanger and Ziotopoulou 2018) constitutive models, respectively. Sensitivity of the computed deformations to the mean horizontal length of the sand-like portions of the interbedded deposit, the cyclic strengths assigned to the sand-like soils, the undrained shear strengths assigned to the clay-like soils, the level of shaking, the water table depth, and other input parameters is evaluated. Newmark sliding block analyses are performed with different allowances for how inter-bedding influences the composite strength of the interbedded stratum. The differences between the results obtained with these various analysis methods, along with those presented by Youd et al. (2009), provide insights on the various factors that can contribute to an over-estimation of ground deformations in interbedded deposits of sands, silts, and clays.

Site Characterization

Site conditions and stratigraphy

Çark Canal, as illustrated by the photograph in Fig. 1 and cross section in Fig. 2, is a channelized segment of the Çark River in Adapazari, Turkey. Youd et al. (2009) showed the canal as 6.5 m deep with 1H:1V side slopes, but the slopes were not directly measured by the site surveyor and the depth of the canal was only estimated because of the swift current at that time (T. L. Youd, personal communication, 2016). Analyses of several photographs of the site taken during reconnaissance and discussion with the original investigators led to the updated geometry shown in Fig. 2 with a channel depth of 4.6 m, water depth of 1 m, and side slopes of 1.8H:1V (Munter et al. 2017). Five CPT soundings, two borings, and a surface wave test were performed to characterize the soils across the canal (Youd et al. 2000). CPTs 1-24 and 1-25 and borings 1-24 and 1-25 are approximately on the section shown in Fig. 2, whereas CPTs 1-23 and 1-22 are located about 38 and 70 m southward parallel to the canal. CPT 1-21 is approximately in line with this section, but is about 62 m westward of CPT 1-22 (i.e., to the left of the limits of Fig. 2).

The three main strata at the site are, as shown on Fig. 2: a surficial fill of predominantly sands and silts about 1 m thick; a stratum of interbedded sands, silts, and clays extending to depths of about 7 m; and an underlying stratum of dense sands. The interbedded stratum is comprised of Holocene fluvial sediments deposited by the meandering Çark and Sakarya rivers (Bray et al. 2000).

The groundwater table at the time of the earthquake is estimated to be at a depth of about 2.6 m away from the canal and closer to a depth of 3.6 m near the canal (i.e., equal to the water level in the canal). The canal liner is assumed to provide little or no resistance to groundwater flow between the canal and surrounding soils for two reasons: (1) the joints in the canal liner at that time were not tightly sealed, as evidenced by plants growing on the canal slopes as shown in Figure 1, and (2) the liner was relatively thin and would have been uplifted and disrupted if pore water pressures in the soil had ever significantly exceeded the water pressures in the canal. The groundwater level away from the canal is more uncertain given the timing and approximate nature of the field measurements; the effect of a shallower or deeper water table depth (i.e., 2.1 to 3.1 m depth) on the NDA results is examined as part of the sensitivity studies presented later.

Profiles of normalized cone tip resistance ($q_{tN} = q_t/P_A$, where P_A = atmospheric pressure) from the CPT soundings are shown in Fig. 3 with the color fill corresponding to Soil Behavior Type Index (I_c) ranges that approximately separate silt mixtures ($I_c \geq 2.6$), sand mixtures ($2.05 \leq I_c < 2.60$) and sands ($I_c < 2.05$) (Robertson 2009). Soils with $I_c < 2.6$ are herein referred to as sand-like, and those with an $I_c \geq 2.6$ as clay-like. The standard correction for pore pressure acting behind the cone tip was not performed because pore pressure measurements were not available for four of the CPTs and the data for the fifth CPT are questionable; the effect of omitting this correction is expected to be minor because the cone pore pressure is likely close to the hydrostatic pressure for the soil and groundwater conditions at this site, and thus it is assumed that the corrected tip resistance q_{tN} is equal to the measured q_{cN}. The cone penetrometer was a standard 10 cm^2 cone. The data show that the surficial fill and the lower sand layer are both dense. The interbedded zone has numerous sand and silty sand lenses ranging from 0.1 to 0.5 m in thickness. This results in the characteristic problem in cone soundings where the q_{tN} gradually transitions up and down in magnitude at every interface. In contrast, the borehole logs (Youd et al. 2000, 2009) report distinct interfaces between alternating strata of CL, ML, SM, and SP soils.

The shear wave velocity (V_s) profile obtained using surface wave techniques shows V_s equal to 220 m/s between depths of 0.0 and 1.0 m, 100 m/s between depths of 1.0 and 3.0 m, 150 m/s between depths of 3.0 and 9.0 m, and 160 m/s between depths of 9.0 and 15.0 m (analyses by Bay and Cox, as reported in Youd et al. 2000). The surface wave techniques provide measurements that are averaged over greater soil volumes than cone penetration resistances are, and hence the shear wave velocity profile does not contain the same degree of detail present in the cone soundings.

Performance in 1999 M=7.5 Kocaeli earthquake

The August 17, 1999 Kocaeli earthquake, with a moment magnitude (M) of 7.5, caused severe damage and liquefaction-related ground failure throughout the city of Adapazari, Turkey located just a few kilometers from the rupture. The single recording of the main shock in the city had a horizontal PGA

of about 0.4 g (Strong Ground Motion Database of Turkey), and peak accelerations throughout the city were likely between 0.3 and 0.5 g (Bray et al. 2000). Post-earthquake reconnaissance near the Çark canal site did not identify evidence of lateral spreading, although several buildings within 100 m of the canal experienced settlements of up to 100 mm (Bray et al. 2000), suggesting that localized liquefaction or cyclic softening occurred.

Correction of CPT data for thin layer and transition zones effects

Thin layer and transition zone effects have been studied extensively using a range of theoretical and experimental methods, although almost exclusively focused on the idealized condition of a uniform strong layer embedded in (or against) a uniform weaker soil; a summary of past studies can be found in Boulanger and DeJong (2018). The layer correction factor (K_H) is the ratio of the true penetration resistance for the stronger layer (q^t_{strong}) without any effects of the surrounding weaker soil divided by the peak penetration resistance "measured" (or mobilized) within the stronger layer (q^m_{peak}). The thin layer factor depends on the ratio of q^t_{strong} to the true penetration resistance for the weaker layer (q^t_{weak}), as illustrated by the results of numerical analyses for a sand lens embedded in soft clay by Ahmadi and Robertson (2005) and Mo et al. (2017), as shown in Figs. 4a and 4b, respectively. The range of K_H values recommended by Youd et al. (2001) based on an examination of field data and the elastic solutions by Vreugdenhil et al. (1994) are also shown in Fig. 4; the basis for this recommended range was not provided, but they are reasonably consistent with the overall trends from experimental and numerical analyses. In general, thin layer factors are close to unity for sand layers greater than about 30 cone diameters (d_c) thick (about 1 m for a 10 cm^2 cone and 1.3 m for a 15 cm^2 cone) and can exceed 2 for strong layers that are less than about 10 d_c thick (about 36 cm for a 10 cm^2 cone and 44 cm for a 15 cm^2 cone). Nonetheless, thin layer correction factors are rarely used in practice because their application to real profiles is subjective, their manual application is time consuming, and the benefits may not be significant enough to warrant the engineering costs.

Boulanger and DeJong (2018) developed an inverse filtering procedure for developing improved estimates of the true tip resistance and sleeve friction values from measured CPT data in interbedded soils. The inverse filtering procedure has three primary components: (1) a model for how the cone penetrometer acts as a low-pass spatial filter in sampling the true distribution of soil resistance versus depth, (2) a solution procedure for iteratively determining an estimate of the true cone penetration resistance profile from the measured profile given the cone penetration filter model, and (3) a procedure for identifying sharp transition interfaces and correcting the data at those interfaces. Application of the inverse filtering procedure to idealized two-layer systems, using the baseline parameters from Boulanger and DeJong (2018), produced the net thin layer factors shown in Fig. 5. These net thin layer factors decrease toward unity as the strong layer thickness becomes progressively thinner than about 4d_c because

the procedure includes low-pass spatial filtering, which is necessary because such high spatial frequencies cannot be inverse filtered reliably given the sampling interval and cone diameter. The inverse filtering procedure was shown to provide an objective, repeatable, and automatable means for correcting cone penetration test data for thin-layer and transition zone effects.

The five CPT soundings after inverse filtering using the procedure and baseline parameters from Boulanger and DeJong (2018) are shown in Fig. 6. For the interbedded stratum, the tip resistances generally increase by 10-100% in the sand and silty sand lenses depending on the lens thickness and decrease by 5-30% in the clay-like soils depending on their proximity to a sand lens.

Properties for the sand-like and clay-like portions of the interbedded zone

Representative properties for the sand-like portion of the interbedded stratum were estimated primarily based on examination of the CPT data. Cumulative distributions of the q_c and I_c values within the interbedded stratum and below the water table are shown for individual CPTs and all CPTs combined, both with and without inverse filtering, in Fig. 7; data from above the water table were excluded because the properties of the liquefiable (and hence saturated) zones are of primary concern. The median q_{cN} increased from about 28 for the measured CPT data to about 49 for the inverse filtered CPT data, which is about a 75% increase. The median I_c decreased from about 2.32 for the measured CPT data to about 2.01 for the inverse filtered CPT data, which is about a 13% decrease. The median FC for the sand-like soils, based on the laboratory test data, ranges from 50-60% depending on which samples are considered sand-like versus clay-like and recognizing that a direct mapping to CPT intervals is uncertain. The median laboratory-based FC is taken as the lower estimate of 50% for the present analyses. The CPT-based liquefaction triggering correlation by Boulanger and Idriss (2015) uses a fines calibration factor C_{FC} to adjust the correlation between I_c and FC; the value of C_{FC} for an individual stratum can be estimated as,

$$C_{FC} = \left(\frac{FC_{median} + 137}{80} \right) - I_{c,median} \tag{1}$$

For the measured CPT data and with the measured FC_{median} taken as 50%, the C_{FC} obtained from the above equation is sufficiently close to zero that the default calibration (with $C_{FC} = 0$) is acceptable. For the inverse filtered data, the estimated C_{FC} is 0.29. The cumulative distributions of the equivalent clean sand, overburden corrected penetration resistance (q_{c1Ncs}) and FC computed from the CPT data using the Boulanger and Idriss (2015) relationships are shown in Figs. 8a and 8b, respectively. The median q_{c1Ncs} increased from about 85 for the measured CPT data to about 115 for the inverse filtered CPT data, which is about a 35% increase. The median FC remains close to 50% for both the measured and inverse filtered CPT data, as expected given their C_{FC} values were calibrated to the laboratory-based value of $FC_{median} = 50\%$.

The q_{c1Ncs} for the sand-like portions of the interbedded stratum are plotted versus depth in Fig. 9 for both the measured and inverse filtered CPT data. The q_{c1Ncs} values are reasonably similar between the five CPTs and are relatively similar over the full thickness of the interbedded stratum.

The undrained shear strength (s_u) of the clay-like portions of the interbedded stratum were first estimated using the CPT data with a cone bearing factor (N_{kt}) of 15. The s_u are plotted versus depth in Fig. 10 for both the measured and inverse filtered CPT data. The s_u are similar between the five CPTs and are also relatively similar over the full thickness of the interbedded stratum. The median s_u from the cumulative distribution for all the CPTs combined decreased from about 56 kPa for the measured CPT data to about 43 kPa for the inverse filtered data, which is a decrease of about 23%. The selection of s_u values for the deformation analyses is complicated by uncertainty in the N_{kt} value used in the CPT interpretation, the effects of increased strain rate during earthquake loading, the selection of representative values from such spatially-variable data, the effects of different loading paths, and other factors. The selection of a baseline value for s_u and sensitivity of the computed deformations to variations in s_u are discussed later.

The interpreted V_s of 150 m/s for most of the interbedded stratum does not differentiate between soil types. This value of V_s appears reasonable for both the sand-like and clay-like soils given their other characteristics, so the same value is used later for modeling both soil types.

One-dimensional Liquefaction Vulnerability Indices

Four one-dimensional (1D) liquefaction vulnerability indices (LVIs) were computed using the measured and inverse filtered CPT data.

- The lateral displacement index (LDI), as named by Zhang et al. (2004), represents a potential maximum lateral ground surface displacement computed by integrating potential maximum shear strains over depth. For the analyses presented herein, the potential maximum shear strains were computed using the relationship by Ishihara and Yoshimine (1992). For level ground conditions away from a free face, Tokimatsu and Asaka (1998) recommended that the dynamic strains for computing dynamic ground lurch can be taken as about 10-20% of the maximum shear strains obtained by the above types of relationships.

- The liquefaction potential index (LPI) developed by Iwasaki et al. (1978) is a depth-weighted function of the factor of safety against liquefaction triggering (FS).

- The one-dimensional reconsolidation settlement (S_{v-1D}) represents a potential ground surface settlement computed by integrating post-liquefaction 1-D reconsolidation strains over depth. For the analyses presented herein, the potential reconsolidation strains were computed using the relationship by Zhang et al. (2002).

- The liquefaction severity number (LSN), introduced by van Ballegooy et al. (2014), is a depth-weighted function of the post-liquefaction 1-D reconsolidation strains, where the potential reconsolidation strains are based on the relationship by Zhang et al. (2002).

All four LVIs were computed using the CPT-based liquefaction triggering correlation by Boulanger and Idriss (2015).

The four LVIs for each of the five CPTs, with and without inverse filtering, are plotted versus PGA in Fig. 11. The LVI values at a PGA of 0.36 g approximately correspond to the 1999 Kocaeli earthquake (i.e., the PGA of the Sakarya recording after processing by Ambraseys et al. 2002), whereas the shapes of the LVI versus PGA curves illustrate their sensitivity to PGA variations and the effect of inverse filtering at different PGA levels. The LDI values at PGA = 0.36 g (Fig. 11a) were reduced from 0.64-1.05 m for the measured CPT data to 0.32-0.58 m for the inverse filtered CPT data, a reduction of about 45-50%. In either case, these relatively large LDI values are inconsistent with the lack of visible ground cracking or deformations at the site. The LPI values at PGA = 0. 36 g (Fig. 11b) were reduced from 5.8-10.7 for the measured CPT data to 3.6-7.3 for the inverse filtered CPT data, for a reduction of about 30-40%. The S_{v-1D} at PGA = 0. 36 g (Fig. 11c) were reduced from 40-76 mm for the measured CPT data to 27-51 mm for the inverse filtered CPT data, for a reduction of about 30-35%. The LSN values at PGA = 0. 36 g (Fig. 11d) were reduced from 8.9-14.1 for the measured CPT data to 5.7-11.7 for the inverse filtered CPT data, for a reduction of about 15-35%. The LPI, S_{v-1D}, and LSN values for the measured CPT data are near the threshold values that approximately distinguish between moderate and minor to no surface manifestation of liquefaction in areas without lateral spreading (e.g., Wotherspoon et al. 2013, Maurer et al. 2014, Tonkin and Taylor 2015, 2016), whereas the values for the inverse filtered CPT data are more consistent with the range associated with minor to no surface manifestation. However, the potential for lateral spreading toward the canal means that the LDI and LPI are more appropriate than either the S_{v-1D} or LSN indices for evaluating potential lateral deformations.

Nonlinear Dynamic Analyses

Two-dimensional NDAs were performed using the numerical platform FLAC 8.0 (Itasca 2016) with stochastic realizations of soil type (i.e., sand-like and clay-like) for the interbedded stratum. The baseline model, shown in Fig. 12, had a 1.5- to 2-m-thick crust, a 4.4- to 5.5-m-thick interbedded stratum, a 3.2- to 3.8-m-thick dense sand base, and a 0.3-m-thick canal liner. The model was 102 m wide and contained about 22,000 zones (or elements), with typical zones in the interbedded stratum being 100 mm thick by 300 mm wide. The water table was imposed as an initial condition on the model. The water table for the baseline model was set at a depth of 2.6 m below the ground surface outside the limits of the canal and varied linearly beneath the canal slopes to meet the water level in the canal (3.6 m below the surrounding ground surface; Fig. 2).

Stochastic realizations

Stochastic realizations for the interbedded stratum were produced using T-PROGS (Transition Probability Geostatistical Software; Carle 1999) which combines transition probabilities, Markov chain modeling, and kriging-based conditional simulation. The transition probability approach represents a spatial correlation structure in categorical systems by describing the probability of transition from one category to another as a function of lag distance. The transition probabilities in the vertical direction obtained from the CPT data for the two-category system of sand-like and clay-like soils are shown in Fig. 13. The results in Fig. 13a show the probability of transitioning from clay-like to sand-like increases from 0 at zero lag distance to about 0.4 at large lag distance. The results in Fig. 13b show the autocorrelation for remaining in sand-like soil at different lag distances. The autocorrelation for clay-like soils and the cross-correlation between sand-like and clay-like soils are not shown because they are the complements of the results shown in Fig. 13. The overall proportion of each category is the transition probability at large lag distance (about 60% for clay-like and 40% for sand-like in this case), and the mean length of each category, which is an index for the average length of an inclusion of that category, is defined as the negative inverse of the slope of auto-transition probability at zero lag distance. Separate transition probability Markov chain models are defined for each orthogonal direction based on field data or geologic understanding. The sand-like proportion was set to 40% and the mean length (L_z) in the vertical direction was set to 0.26 m. Transition probabilities in the horizontal (cross-channel) direction cannot be determined from the widely spaced CPTs, so instead a range of horizontal mean lengths (L_x) for the sand-like soils were estimated based on site's depositional setting. The interbedded stratum was formed by fluvial depositional processes (e.g., overbank flooding, river meandering, side streams, and surface flows) associated with a river up to about 10 m wide; therefore L_x values of 5, 10, and 40 m for the sand-like soils were examined. Finally, a kriging-based approach was used to produce a set of stochastic realizations for each set of transition probability parameters using the defined Markov chain models in the horizontal and vertical directions and conditioned on the sand-like and clay-like layering in the CPT 1-24 and 1-25 soundings.

Constitutive model calibrations

The sand-like portions of the interbedded deposit, plus the fill and underlying dense sand layer, were modeled using the constitutive model PM4Sand version 3.1 (Ziotopoulou and Boulanger 2016, Boulanger and Ziotopoulou 2017), with the model parameters listed in Table 2. For the sand-like soils in the interbedded stratum, calibrations were developed for representative q_{c1Ncs} values of 85 and 115, which correspond to $CRR_{M7.5,\sigma=1}$ values of 0.12 and 0.16, respectively, based on the triggering correlation by Boulanger and Idriss (2015). These representative q_{c1Ncs} values approximately correspond to the median values for the measured and inverse filtered CPT data, with the median value appearing to be a reasonable

percentile for evaluating lateral spreading displacements of gently sloping ground with a uniform analysis model (Montgomery and Boulanger 2016). The shear modulus coefficient (G_o) was set to 585 for both calibrations to match the in-situ V_s at the middle of the stratum, the apparent relative density (D_R) was estimated as 48 and 61% using the relationships in Idriss and Boulanger (2008), and the contraction rate parameter (h_{po}) was iteratively adjusted to obtain the target cyclic strength in 15 uniform cycles of undrained direct simple shear (DSS) loading. Default values were used for all other, secondary parameters. The calibration process for the underlying saturated dense stratum and overlying fill was the same, although the fill soils are not susceptible to liquefaction because they are unsaturated. Examples of element responses with these types of values are shown in Boulanger and Ziotopoulou (2017).

The clay-like portions of the interbedded deposit were modeled using the constitutive model PM4Silt (Boulanger and Ziotopoulou 2018) with the model parameters listed in Table 3. The first calibration, which is used for all baseline analyses, was based on an in-situ s_u of 35 kPa, which was selected as being representative of weaker zones at various elevations (Fig. 10) and corresponds approximately to the 33rd percentile of the s_u values derived from the inverse filtered CPT data. The second calibration, used in sensitivity analyses, was based on an in-situ s_u of 44 kPa (about 25% greater than 35 kPa), which is closer to the median value for the inverse filtered CPT data (or about the 33rd percentile for the measured CPT data). These s_u values are considered applicable for static loading applications, whereas the required input parameter for PM4Silt in an NDA is the s_u at critical state for earthquake loading rates ($s_{u,cs,eq}$). Accordingly, the $s_{u,cs,eq}$ values listed in Table 3 include a 25% increase for strain rate effects relative to the CPT-derived s_u values. The G_o was set to 585 to match the in-situ V_s at the middle of the layer. The shear modulus reduction (G/G_{max}) and equivalent damping behavior was close to those recommended by Vucetic and Dobry (1991) for fine-grained soil with a PI of about 15, so the shear modulus parameter (h_o) was left at its default value of 0.5. The h_{po} was adjusted to produce reasonable slopes for the cyclic strength curves in undrained DSS loading as shown in Fig. 14. Default values were used for all other, secondary parameters. Cyclic strength curves for the baseline calibrated model are shown for initial σ'_{vo} of 40 and 100 kPa, illustrating the dependence of cyclic strength on σ'_{vo} when $s_{u,cs}$ is a constant. Examples of the stress-strain responses for these two overburden stresses are shown in Fig. 15.

The canal liner was modeled using a Mohr Coulomb model with a friction angle of 39 degrees, cohesion intercept of 10 kPa, shear modulus of 25 MPa, and Poisson's ratio of 0.3.

Input motion and dynamic analysis conditions

The input motion time history was the east-west outcrop recording of the Kocaeli earthquake from the Sakarya station with a PGA of about 0.41 g before processing (Strong Ground Motion Database of Turkey) and a PGA of about 0.36 g after processing by Ambraseys et al. (2002). This recording station is

located about 4 km south of the Çark Canal site, is founded on stiff soils, and did not record the north-south component of the motion. The input motion was imposed as a stress time series to the compliant base of the model. The side boundaries of the model were attached; sensitivity studies with larger distances to the lateral boundaries confirmed that the boundaries are sufficiently far from the canal to not influence deformations near the canal.

The dynamic analyses were performed with no seepage allowed during shaking; seepage was included in the static stress initialization, but turned off for the dynamic analysis because drainage is expected to be negligible for these types of soils during dynamic loading. Rayleigh damping of 0.5% at a frequency of 5 Hz was specified. All analyses assume small deformations; sensitivity studies confirmed this is reasonable for the magnitude of deformations that develop. Sensitivity analyses using reduced time step sizes confirmed that convergence was obtained using FLAC's default time step sizes.

Simulation results

Results for one of the simulations with the interbedded stratum modeled using L_x = 10 m and q_{c1Ncs} = 115 for the sand-like portion are illustrated in Fig. 16, which shows the stratigraphy for this realization, contours of maximum shear strains, and contours of horizontal displacements at the end of shaking. Almost all of the sand-like soils reach a peak excess pore pressure ratio of 100% or develop shear strains in excess of 3% during shaking, depending on their location relative to the canal. The largest shear strains develop in the longer lenses of sand-like soils that coalesce as part of a mechanism for lateral spreading of each slope toward the canal. The shear strains in the clay-like soil portions are generally much smaller than in the sand-like portions, which is expected given the clay-like portions have greater cyclic strength throughout the stratum. Lateral displacements of the slope are greatest near the canal and decrease with distance from the canal. Lateral ground surface displacements at points located 2 m from the head of each slope are about 87 mm on the west side and about 62 mm on the east side. Ground surface settlements at these same points are about 33 mm and 29 mm on the west and east sides, respectively, or about 38-47% of the lateral displacements.

The differences in lateral displacements on the east and west sides of the canal are largely attributed to the input motion characteristics because repeating the analysis with the input motion polarity reversed results in the lateral displacements at a point 2 m from the head of each side slope becoming 68 mm (versus 87 mm) on the west side and 80 mm (versus 62 mm) on the east side. The lateral displacements on the west side still tend to be slightly greater than on the east side, even after accounting for input motion polarity, which may be attributed to systematic differences in the stratigraphy near the slopes (e.g., crust thickness; proportion of sand-like soils below the water table; lateral continuity of sand-like lenses) that reflect the realizations being conditioned on CPT soundings 1-24 (west side) and 1-25 (east side).

Results for one of the simulations with the sand-like portions of the interbedded stratum having the larger L_x of 40 m are shown in Fig. 17. The simulated stratigraphy tends to have longer lenses of sand-like soils, as expected, but also tends to have fewer lenses because the overall proportion is still controlled by the defined sill (i.e., 40% sand-like). The greatest shear strains again develop along the sand-like soils, and the overall mechanisms for lateral spreading on both sides of the canal are similar to those shown in Fig. 16. Lateral displacements of the slopes, at a point 2 m from the head of the slope, are about 87 mm on the west side and about 59 mm on the east side. The lateral spreading displacements for the cases shown in Figs. 16 and 17 are similar despite their differences in the L_x for the sand-like portions of the interbedded stratum; the similar displacements are attributed to the lateral spreading mechanism being concentrated near the slopes, the two realizations having the same sills, and the two realizations being conditioned on the same CPTs located on either side of the canal.

The lateral displacements on the canal banks are plotted in Fig. 18 versus L_x for the various realizations and the baseline constitutive model calibrations (q_{c1Ncs} = 85 for the sand-like portions; s_u = 35 kPa for the clay-like portions). These results show that the lateral displacements on the west and east banks did not vary significantly between realizations or between L_x values of 5, 10 or 40 m. The small dispersion in lateral displacement between realizations means that a relatively small number of realizations were necessary to obtain the mean responses. The insensitivity of the lateral displacements to L_x or variations between realizations is consistent with the factors discussed previously.

Repeating the above analyses with the calibration of PM4Sand based on q_{c1Ncs} = 85 for the sand-like portions of the interbedded stratum resulted in lateral displacements increasing to 180-200 mm on the west bank and 120-150 mm on the east bank, which are about 2.3-2.5 times greater than when the calibration was based q_{c1Ncs} = 115. These larger lateral displacements are inconsistent with the lack of visible damage at the site, which indicates that these NDAs over-estimate ground deformations when the calibration is based on measured CPT data without corrections for thin layer and transition effects.

An additional set of analyses was performed using the second PM4Silt calibration listed in Table 3, which used a $s_{u,cs,eq}$ value for the clay-like portion of the interbedded zone that was 25% greater than the first calibration. This set of analyses used the models with L_x = 10 m and q_{c1Ncs} = 115 for the sand-like portion of the interbedded zone. The increased $s_{u,cs,eq}$ resulted in less than 2% reductions in lateral displacements for both banks of the canal. The small effect of increasing the $s_{u,cs,eq}$ is attributed to the fact that most of the deformations result from shear strains in the saturated sand-like soils and the full shear strength of the clays is not being mobilized throughout the stratum at these levels of deformation. The effect of changing $s_{u,cs,eq}$ would likely have been greater if smaller $s_{u,cs,eq}$ values had been used, perhaps based on using a larger N_{kt} value and/or neglecting strain rate effects, but the range of $s_{u,cs,eq}$ values covered in the present analyses was considered reasonable and sufficient for the present study.

Sets of analyses using the realizations with $L_x = 10$ m and $q_{c1Ncs} = 115$ for the sand-like portion of the interbedded zone were repeated with modified input motions to evaluate their effects on computed displacements. One set of analyses used the same input motion, linearly scaled up or down by 20% (i.e., outcrop PGAs of 0.289 and 0.433 g) as a qualitative allowance for uncertainty in the actual site motions. The lateral displacements at 2 to 5 m from the head of the slope on both banks increased by 48-59% for the larger PGA and decreased by 23-39% for the smaller PGA. A second set of analyses used the processed Sakarya station recording from the Strong Ground Motion Database of Turkey. This record had a PGA of 0.417 g (about 15% greater than the record processed by Ambraseys et al. 2002) because a wider filter bandwidth was used (0.03-40 Hz versus 0.25-25 Hz) which removed less of the high and low frequencies. The lateral displacements on both banks only increased by 4-9% for this input motion versus the motion by Ambraseys et al. (2002); the effect on lateral displacements was relatively small because these two motions are very similar except at the highest and lowest frequencies. Uncertainty in the actual motions at the site are an unavoidably significant source of uncertainty in the computed displacements, but this uncertainty applies to all analysis approaches and does not appear to change the general observations drawn from comparing the different analysis results.

Sets of analyses using the realizations with $L_x = 10$ m and $q_{c1Ncs} = 115$ for the sand-like portion of the interbedded zone were also repeated with the groundwater table away from the canal raised 0.5 m (i.e., water table depth of 2.1 m) and lowered 0.5 m (i.e., water table depth of 3.1 m). For either groundwater table depth away from the canal, the water table still varied linearly beneath the canal slopes to meet the water level in the canal. The higher water table away from the canal caused the lateral ground displacements at 2 to 5 m from the head of the slope on both sides of the canal to increase by 5-9%, whereas the lower water table caused them to decrease by 7-9%. These results indicate that the computed deformations are not sensitive to the water table levels away from the canal, perhaps because groundwater levels closer to the canal are tied to water level in the canal itself and this range of water table variations did not significantly change the amount of liquefiable soils that remained saturated near the canal.

Newmark sliding block analyses

Newmark sliding block analyses by Youd et al. (2009) predicted negligible displacements based on the assumption that the shear strength of the interbedded stratum was equal to the 42-43 kPa undrained shear strength they estimated for the clay-like portions alone. This analysis case did not account for strength loss in the sand-like portions of the interbedded stratum and was based on a different canal geometry as discussed previously.

Horizontal seismic yield coefficients for different failure masses were obtained from limit equilibrium slope stability analyses using the Spencer (1967) method. The interbedded stratum was modeled as a series of horizontally stratified layers that alternated between sand-like and clay-like soils, with the total

thickness of the sand-like layers comprising 40% of the stratum (i.e., equal to the sill value). The clay-like portion was assigned an undrained shear strength of 43 kPa, which is approximately the 50th percentile value and implicitly assumes that the effects of increased strain-rate and cyclic degradation are offsetting. The sand-like portions below the water table were modeled as having an undrained (residual) shear strength ratio (S_r/σ'_{vo}) of 0.11 based on the inverse filtered CPT data and the results of case history back-analyses by Olson and Johnson (2008). The sand-like portion above the water table and the fill layer were modeled as having drained strengths with an effective friction angle of 36 degrees. Three cases were considered for the shear strength along horizontal failure planes: (1) the strength is equal to that of the sand-like soil, (2) the strength is a composite based on 80% of the surface passing through sand-like soil and 20% passing through clay-like soils, and (3) the strength is a composite based on 60% of the surface passing through sand-like soils and 40% passing through clay-like soils. Horizontal seismic yield coefficients for slip surfaces that day-light 2-6 m away from the edge of the canal slope were 0.11, 0.21, and 0.33 for these three cases, respectively.

Newmark displacements for the above yield coefficients were computed using the regression model by Bray and Travasarou (2007) for the coupled response of a slide mass with a single mode shape. The degraded period of the slide mass was estimated to be about 0.18 s, for which the 5%-damped elastic spectral acceleration is about 0.85 g based on the outcrop motion used for the NDAs. The liquefiable soils were assumed to liquefy early in strong shaking. Newmark displacements for the above yield coefficients had expected values of 350 mm (180-670 mm for plus/minus one standard deviation) for the first analysis case, 120 mm (60-230 mm) for the second analysis case, and 47 mm (24-91 mm) for the third analysis case. Repeating these analyses with the liquefied soils' strengths based on the measured CPT data (rather than inverse filtered data), increased the expected displacements to 500, 140, and 51 mm, respectively; the increase being larger when the percentage of sand-like soils along the horizontal plane is assumed to be larger. In all cases, these displacements are greater than estimated by Youd et al. (2009) because they include allowances for strength loss in the sand-like portions of the interbedded stratum. The expected displacements from the first Newmark analysis case are several times those obtained from the NDAs, which is consistent with the more conservative assumption that strengths along the horizontal failure planes are entirely controlled by liquefied sand-like soils. The expected displacements from the third analysis case are comparable to those obtained from the NDAs and are in the range expected given the observed lack of damage at the site, but the strength assumptions for this analysis case are difficult to justify based on the available site characterization data and common practices. Nonetheless, these results illustrate that: (1) the expected lateral displacements are sensitive to assumptions regarding the spatial distribution and horizontal continuity of clay-like and sand-like soils within the interbedded stratum and

(2) the assumption of horizontal continuity for the sand-like layers will contribute to conservative estimates of deformations.

Discussion

The absence of visible damage at Çark Canal suggests that lateral displacements along the banks of the canal were likely less than about 50-75 mm near the edges of the canal (i.e., an amount that the unfinished surfaces might accommodate without visible cracking) and likely less than about 25-40 mm at distances more than 5 m from the canal (i.e., an amount that the residential structures might accommodate without visible cracking). These thresholds are subjective, but are considered reasonable given observations from earthquake reconnaissance studies for a range of site conditions.

The LDI, NDA, and Newmark analysis methods all over-predict lateral displacements at the Çark Canal to different degrees for certain assumptions and practices common in industry. The use of the measured CPT data without corrections for thin layer and transition effects increased the degree of over-prediction, or led to over-predictions, for all three analysis methods. The assumption of horizontally continuous liquefied sand lenses in the interbedded stratum, which is inherent to LDI methods and was one assumption scenario for the Newmark analyses, also contributes to conservative estimates of lateral displacements. Empirical estimates using the multiple linear regression (MLR) model of Youd et al. (2002) similarly over-estimated the potential lateral displacements; i.e., Youd et al. (2009) computed lateral displacements of 0.7-2.6 m at a distance of about 25 m from the edge of the canal, with even larger displacements expected closer to the canal.

More realistic estimates of lateral displacements at the canal were provided by the NDAs and Newmark analyses when the properties were based on the inverse filtered CPT data and allowance was made for the spatial variability of the sand-like and clay-like portions of the interbedded stratum (explicitly in the NDAs and indirectly in the Newmark analyses). The stochastic realizations for the interbedded stratum demonstrate that the uncertainty in the spatial correlation parameters did not strongly affect the resulting deformations, whereas guidance on how to incorporate these effects in a Newmark analysis are not well developed. Other factors that might have contributed to smaller displacements in the field include the potential for partially saturated conditions existing below the water table, conservative bias in the CPT-based correlations used to deterministically estimate the cyclic strengths or cyclic mobility behaviors for silty sands and sandy silts, the restraining effects of the bridge across the canal, and uncertainty in the presence and thickness of stronger base soils beneath the canal liner.

Conclusions

The seismic performance of Çark Canal in the 1999 M=7.5 Kocaeli earthquake was evaluated using LVI, NDA, and Newmark sliding block analysis methods, which complement previous analyses by Youd et al. (2009) using an empirical MLR lateral spreading model and a Newmark sliding block approach. The

results of these analyses provide insight into how various factors can contribute to an over-estimation of liquefaction effects in interbedded deposits by different analysis approaches.

The characterization of the interbedded fluvial stratum based on CPT data was revisited using the inverse filtering procedure developed by Boulanger and DeJong (2018) to correct the CPT data for thin layer and transition zone effects. Inverse filtering of the CPT data, combined with a site-specific calibration to the fines content from adjacent borings, increased the representative q_{c1Ncs} values for the sand-like portions of the interbedded stratum by about 35% and decreased the representative undrained shear strengths for the clay-like portions by about 23%.

Common LVIs were computed using the measured and inverse filtered CPT data with the site-specific FC calibration to show that the combination of these two steps reduced the LVIs by 30-50% for this site and seismic loading. The LPI, LSN, and $S_{v\text{-}1D}$ indices for the inverse filtered CPT data were in the ranges associated with minor to no expected damage for areas without the potential for lateral spreading, which is appropriate for areas located some reasonable distance from the canal. The LDI procedure used herein estimated lateral displacements of 0.33-0.60 m, which greatly exceed the range of possible displacements that might have occurred without visible cracking or other damage near the slopes. The LDI's over-estimation of lateral displacements is attributed primarily to the inherent limitations of the analysis method itself, rather than to the possible variations in the components of the analysis (e.g., alternative correlations for cyclic strength or maximum shear strains).

Two-dimensional NDAs were performed using a transition probability approach to generate stochastic realizations for the interbedded stratum and the measured and inverse filtered CPT data to estimate properties. The lateral displacements near the canal banks were over-predicted when properties of the sand-like soils were based on the measured CPT data (i.e., 120-200 mm) but were consistent with minor to no visible damage when the properties were based on the inverse filtered CPT data (e.g., 60-90 mm).

Newmark sliding block analyses over-predicted lateral displacements when the liquefiable sand-like portions of the interbedded stratum were assumed horizontally continuous, regardless of whether their properties were based on measured or inverse filtered CPT data (i.e. ≥ 350 mm). Newmark displacements were consistent with the absence of visible damage when horizontal failure planes were assumed to pass through at least 40% clay-like soil and the properties of the sand-like soils were based on inverse filtered CPT data.

The tendency for common liquefaction evaluation procedures to overestimate liquefaction effects in interbedded deposits is attributed to the cumulative effects of various limitations in the site characterization tools, correlations, and analysis procedures (Table 1). The role of each limitation depends on the specific site and seismic loading conditions. The improved prediction of lateral spreading

displacements using an NDA or Newmark method relative to LDI or MLR procedures, for this case history, is attributed to their more realistic representations of site geometry and stratigraphy and, in the case of the NDAs, the direct modeling of the dynamic response.

Acknowledgments

References

Ahmadi, M. M. and Robertson, P. K. (2005). "Thin-layer effects on the CPT q_c measurement." Canadian Geotechnical Journal, 42(5), 1302-1317.

Ambraseys, N., Smit, P., Sigbjornsson, R., Suhadolc, P. & Margaris, B. (2002). Internet-Site for European Strong-Motion Data, European Commission, Research-Directorate General, Environment and Climate Programme.

Beyzaei, C. Z., Bray, J. D., Cubrinovski, M., Riemer, M., and Stringer, M. E. (2018). "Laboratory-based characterization of shallow silty soils in southwest Christchurch." Soil Dynamics and Earthquake Engineering, 110: 93-109.

Boulanger, R. W., and DeJong, J. T. (2018). "Inverse filtering procedure to correct cone penetration data for thin-layer and transition effects." Proc., Cone Penetration Testing 2018, Hicks, Pisano, and Peuchen, eds., Delft University of Technology, The Netherlands, 25-44.

Boulanger, R. W., and Ziotopoulou, K. (2018). "PM4Silt (Version 1): A silt plasticity model for earthquake engineering applications." Report No. UCD/CGM-18/01, Center for Geotechnical Modeling, Dept. of Civil and Environmental Engrg., University of California, Davis, CA, 108 pp.

Boulanger, R. W., and Ziotopoulou, K. (2017). "PM4Sand (Version 3.1): A sand plasticity model for earthquake engineering applications." Report No. UCD/CGM-17/01, Center for Geotechnical Modeling, Dept. of Civil and Environmental Engrg., University of California, Davis, CA, 113 pp.

Boulanger, R. W., Moug, D. M., Munter, S. K., Price, A. B., and DeJong, J. T. (2016). "Evaluating liquefaction and lateral spreading in interbedded sand, silt, and clay deposits using the cone penetrometer." Geotechnical and Geophysical Site Characterisation 5, B. M. Lehane, H. Acosta-Martinez, and R. Kelly, eds., Australian Geomechanics Society, Sydney, Australia, ISBN 978-0-9946261-2-7.

Boulanger, R. W., & Idriss, I. M. (2015). "CPT-Based Liquefaction Triggering Procedure." Journal of Geotechnical and Geoenvironmental Engineering, 142(2), 04015065.

Bray, J. D., Stewart, J. P., Baturay, M. B., Durgunoglu, T., Onalp, A., Sancio, R. B., Ural, D., Ansal, A., Bardet, J. B., Barka, A., Boulanger, R. W., Cetin, O., & Erten, D. (2000). "Damage patterns and foundation performance in Adapazari." Earthquake Spectra, 16(S1), 163-189.

Bray, J. D., and Travasarou, T. (2007). "Simplified procedure for estimating earthquake-induced deviatoric slope displacements." J. Geotechnical and Geoenvironmental Engineering, 133(4): 381-392.

Carle, S. F. (1999). T-PROGS: Transition probability geostatistical software. University of California, Davis, CA.

Chu, D. B., Stewart, J. P., Youd, T. L. & Chu, B. L. (2007). "Liquefaction-induced lateral spreading in near-fault regions during the 1999 Chi-Chi, Taiwan Earthquake." J. Geotechnical and Geoenvironmental Engineering, ASCE, 132(12), 1549-1565.

Idriss, I. M. and Boulanger, R. W. (2008). Soil liquefaction during earthquakes. Monograph MNO-12, Earthquake Engineering Research Institute, Oakland, CA, 261 pp.

Ishihara, K. and Yoshimine, M. (1992). "Evaluation of settlements in sand deposits following liquefaction during earthquakes." Soils and Foundations, Japanese Geotechnical Society, 32(1): 173-188.

Itasca (2016). "FLAC, Fast Lagrangian Analysis of Continua, User's Guide, Version 8.0." Itasca Consulting Group, Inc., Minneapolis, MN.

Iwasaki, T., Tatsuoka, F., Tokida, K., and Yasuda, S. (1978). "A practical method for assessing soil liquefaction potential based on case studies at various sites in Japan." Proceedings of the 2nd International Conference on Microzonation, Nov 26-Dec 1, San Francisco, CA, USA.

Maurer, B.W., Green, R.A., Cubrinovski, M. and Bradley, B.A. (2014). "Evaluation of the Liquefaction Potential Index for Assessing Liquefaction Hazard in Christchurch, New Zealand." J. Geotechnical and Geoenvironmental Engineering, ASCE, 140(7): 04014032, 10.1061/(ASCE)GT.1943-5606.0001117.

Mo, P.-Q., Marshall, A. M., and Yu, H.-S. (2017). "Interpretation of cone penetration test data in layered soils using cavity expansion analysis." J. Geotechnical and Geoenvironmental Eng., 143(1), 10.1061/(ASCE)GT.1943-5606.0001577.

Montgomery, J., and Boulanger, R. W. (2016). "Effects of spatial variability on liquefaction-induced settlement and lateral spreading." J. Geotechnical and Geoenvironmental Engineering, ASCE, 2017, 143(1), 04016086, 10.1061/(ASCE)GT.1943-5606.0001584.

Munter, S. K., Boulanger, R. W., Krage, C. P., and DeJong, J. T. (2017). "Evaluation of liquefaction-induced lateral spreading procedures for interbedded deposits: Çark Canal in the 1999 M7.5 Kocaeli

earthquake." Geotechnical Frontiers 2017, Seismic Performance and Liquefaction, Geotechnical Special Publication No. 281, T. L. Brandon and R. J. Valentine, eds., 254-266.

Olson, S. M., & Johnson, C. I. (2008). "Analyzing liquefaction-induced lateral spreads using strength ratios." J. Geotechnical and Geoenvironmental Engineering, 134(8), 1035-1049.

Robertson, P. K. (2009). "Interpretation of cone penetration tests – a unified approach." Canadian Geotechnical Journal, 46, 1337-1355.

Spencer, E. (1967). "A method of analysis of the stability of embankments assuming parallel inter-slice forces." Geotechnique, 17(1), 11-26.

Strong Ground Motion Database of Turkey. Earthquake Research Department, General Directorate of Disaster Affairs, Republic of Turkey. http://kyhdata.deprem.gov.tr (accessed October 2016).

Tokimatsu, K., and Asaka, Y. (1998). "Effects of liquefaction-induced ground displacements on pile performance in the 1995 Hyogoken-Nambu earthquake." Special Issue of Soils and Foundations, Japanese Geotechnical Society, 163-177.

Tonkin and Taylor Ltd. (2015). Canterbury Earthquake Sequence: Increased Liquefaction Vulnerability Assessment Methodology. Chapman Tripp acting on behalf of the Earthquake Commission (EQC), Tonkin & Taylor ref. 52010.140.v1.0.

Tonkin and Taylor Ltd. (2016). Practical implications of increased liquefaction vulnerability. Chapman Tripp acting on behalf of the Earthquake Commission (EQC), Tonkin & Taylor ref. 52010.140.v2.0 0032-4-R-CPE-2016.

van Ballegooy, S., Malan, P., Lacrosse, V., Jacka, M. E., Cubrinovski, M., Bray, J. D., O'Rourke, T. D. O., Crawford, S. A. and Cowan, H. (2014). "Assessment of liquefaction-induced land damage for residential Christchurch." Earthquake Spectra, EERI, 30(1), 31-55.

Vreugdenhil, R., Davis, R. and Berrill, J. (1994). "Interpretation of cone penetration results in multilayered soils." International Journal of Numerical and Analytical Methods in Geomechanics, 18(9), 585-599.

Vucetic, M., and Dobry, R. (1991). "Effect of soil plasticity on cyclic response." J. Geotechnical Engineering, 117(1): 89-107.

Wotherspoon, L., Orense, R., Green, R., Bradley, B., Cox, B., & Wood, C. (2013). "Analysis of liquefaction characteristics at Christchurch strong motion stations." Proceedings, New Zealand – Japan Workshop on Soil Liquefaction during Recent Large-Scale Earthquakes, Auckland, New Zealand, December.

Youd, T. L., DeDen, D. W., Bray, J. D., Sancio, R., Cetin, K. O., & Gerber, T. M. (2009). "Zero-displacement lateral spreads, 1999 Kocaeli, Turkey, earthquake." Journal of Geotechnical and Geoenvironmental engineering, 135(1), 46-61.

Youd, T. L., Hansen, C. M., & Bartlett, S. F. (2002). "Revised multilinear regression equations for prediction of lateral spread displacement." J. Geotechnical and Geoenvironmental Engineering, 128(12), 1007-1017.

Youd, T. L. et al. (2001). "Liquefaction resistance of soils: Summary report from the 1996 NCEER and 1998 NCEER/NSF Workshops on Evaluation of Liquefaction Resistance of Soils." J. Geotechnical and Geoenvironmental Engineering, 127(4), 297–313.

Youd, T. L., Cetin, K. O., Bray, J. D., Seed, R. B., Durgunoglu, H. T., and Onalp, A. (2000). "Geotechnical site investigation at lateral spread sites." https://apps.peer.berkeley.edu/publications/turkey/adapazari/phase4/index.html (accessed July 22, 2018).

Zhang, G., Robertson, P. K., & Brachman, R. W. I. (2004). "Estimating liquefaction-induced lateral displacements using the standard penetration test or cone penetration test." J. Geotechnical and Geoenvironmental Engineering, 130(8), 861-871.

Zhang, G., Robertson, P.K. and Brachman, R.W.I. (2002). "Estimating liquefaction-induced ground settlements from CPT for level ground." Canadian Geotechnical Journal, 39: 1168-1180.

Ziotopoulou, K., & Boulanger, R. W. (2016). "Plasticity modeling of liquefaction effects under sloping ground and irregular cyclic loading conditions." Soil Dynamics and Earthquake Engineering, 84 (2016), 269-283, 10.1016/j.soildyn.2016.02.013.

Table 1. Factors affecting prediction of liquefaction effects in interbedded soil deposits (after Boulanger et al. 2016)

Factor	Description of role
Limitations in site characterization tools and procedures	
Interface transitions	Penetration resistance (e.g., q_t) in sand is reduced near interfaces with clays or silts. I_c values increase in the sandy soils and decrease in the clays/silts near the interface.
Thin layer effects	Penetration resistance (e.g., q_t) reduced throughout sand layers less than about 1 m thick (with clays/silts on either side of the layer).
Graded bedding	In-situ tests measurements may not differentiate between material transitions that occur across distinct interfaces (e.g., erosional contacts) and material transitions that are gradual (e.g., beds with normal or reverse grading, or bed series in fining-upward or coarsening-upward patterns). Transition and thin layer effects in interbedded soils with graded bedding are not well-understood.
Continuity of lenses	Large horizontal spacing of explorations may not enable the lateral continuity of weak or liquefiable layers to be evaluated or quantified.
Saturation	Presumption of 100% saturation below the groundwater table may underestimate cyclic strengths for partially saturated zones.
Limitations in correlations for liquefaction triggering or consequences	
Triggering	Triggering correlations are not well-constrained for intermediate soils with certain FC and PI combinations; CRR likely underestimated if treated as sand-like, and overestimated if treated as clay-like. Effects of age, stress & strain history, K_o, and cementation not explicitly accounted for.
Strains	Correlations for estimating shear and volumetric strains have been developed primarily from data for sands or clays; the applicability of these correlations for intermediate soils is uncertain.
Limitations from analysis approaches and neglected mechanisms	
Spatial variability	The assumption that liquefiable layers are laterally continuous can contribute to over-estimation of potential liquefaction effects. Composite strength from non-liquefied and liquefied zones may limit deformations.
Thick crust layers	Thick crust layers can reduce surface manifestations of liquefaction at depth in areas without lateral spreading.
Dynamic response	Liquefaction of loose layers in one depth interval may reduce seismic demand on soils in other depth intervals.
Diffusion	Seepage driven by excess pore pressures may increase or decrease ground deformations depending on stratigraphy, permeability contrasts, geometry, seismic loading, and other factors.
Geometry & scale	The 2D or 3D geometry of a deformation mechanism affects the dynamic response and role of spatial variability.

Table 2. Input parameters for PM4Sand

Input parameter [a]	Sand-like portion of interbedded stratum		Surficial fill	Underlying dense stratum
	$q_{c1Ncs}=85$	$q_{c1Ncs}=115$		
D_R – apparent relative density	48%	61%	82%	99%
G_o – shear modulus coefficient	585	585	600	630
h_{po} – contraction rate parameter	0.40	0.28	1.0	1.0

[a] Default values were used for all secondary parameters as listed in Boulanger and Ziotopoulou (2017)

Table 3. Input parameters for PM4Silt

Input parameter [a]	Clay-like portion of interbedded stratum	
	In-situ $s_u = 35$ kPa [b]	In-situ $s_u = 44$ kPa [b]
$s_{u,cs,eq}$ – s_u at critical state for earthquake loading rates	44 kPa	55 kPa
G_o – shear modulus coefficient	585	585
h_{po} – contraction rate parameter	100	100

[a] Default values for all secondary parameters as listed in Boulanger and Ziotopoulou (2018)
[b] In-situ s_u for static loading applications

Figure 1. A south-to-north view of Çark bridge from the west bank of Çark canal in August 2000 (courtesy Brady Cox)
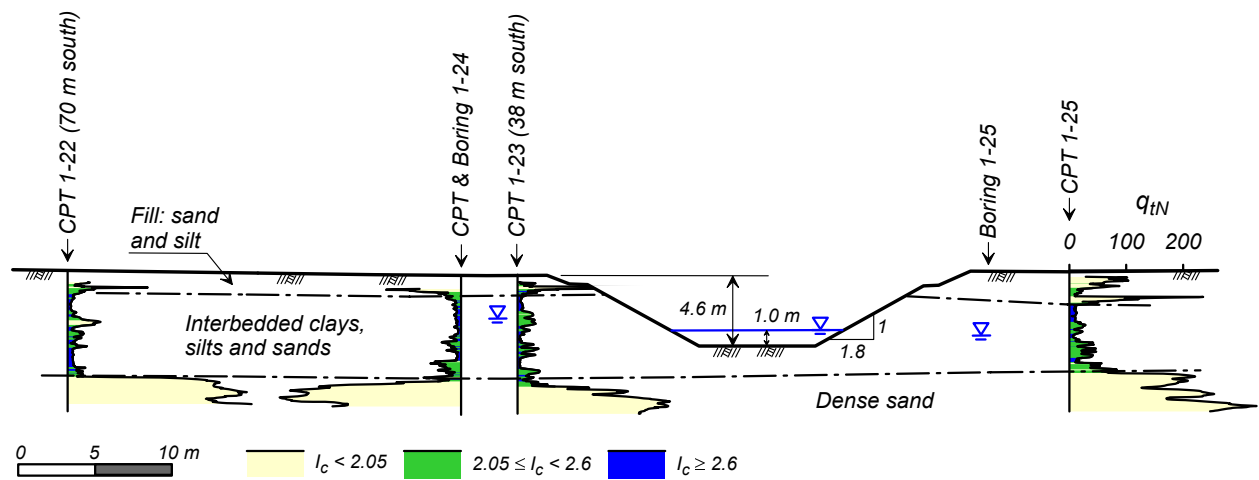
Figure 2. Cross section of canal showing CPT profiles (data from Youd et al. 2009) and updated geometry (Munter et al. 2017); CPTs 1-22 and 1-23 are projected northward parallel to the canal onto this section, whereas CPT 1-21 is located in-line with this section and about 62 m westward of CPT 1-22 (i.e., to the left of the limits of this section).
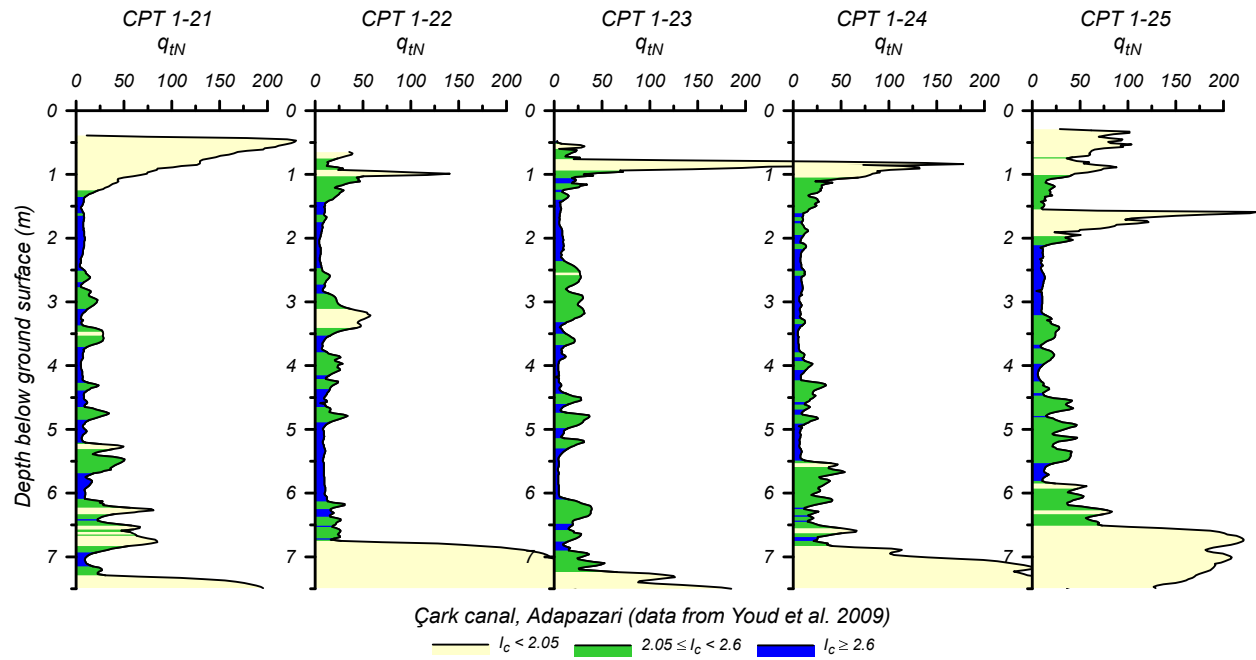
Figure 3. Cone penetration test profiles (data from Youd et al. 2000)
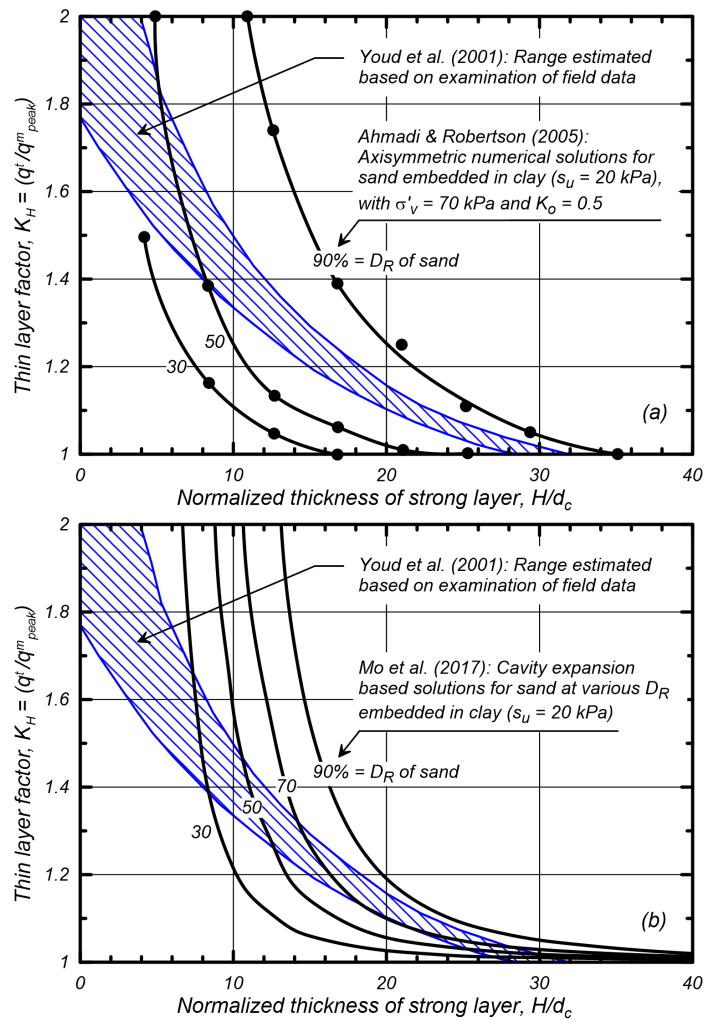
Figure 4. Thin layer correction factors inferred from field data (Youd et al. 2001) compared to: (a) axisymmetric numerical analyses by Ahmadi and Robertson (2005), and (b) cavity-expansion-based solutions by Mo et al. (2017)
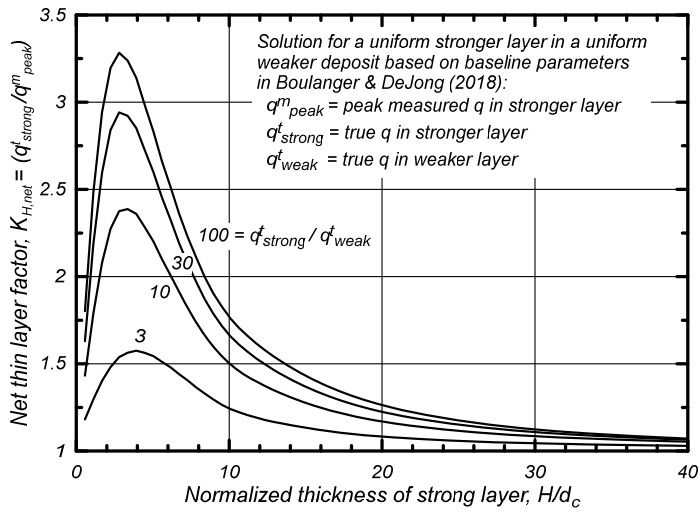
Figure 5. Thin layer correction factors derived by applying the inverse filtering procedure of Boulanger and DeJong (2018) with their baseline parameters to an idealized profile of a uniform stronger layer in a uniform weaker deposit.
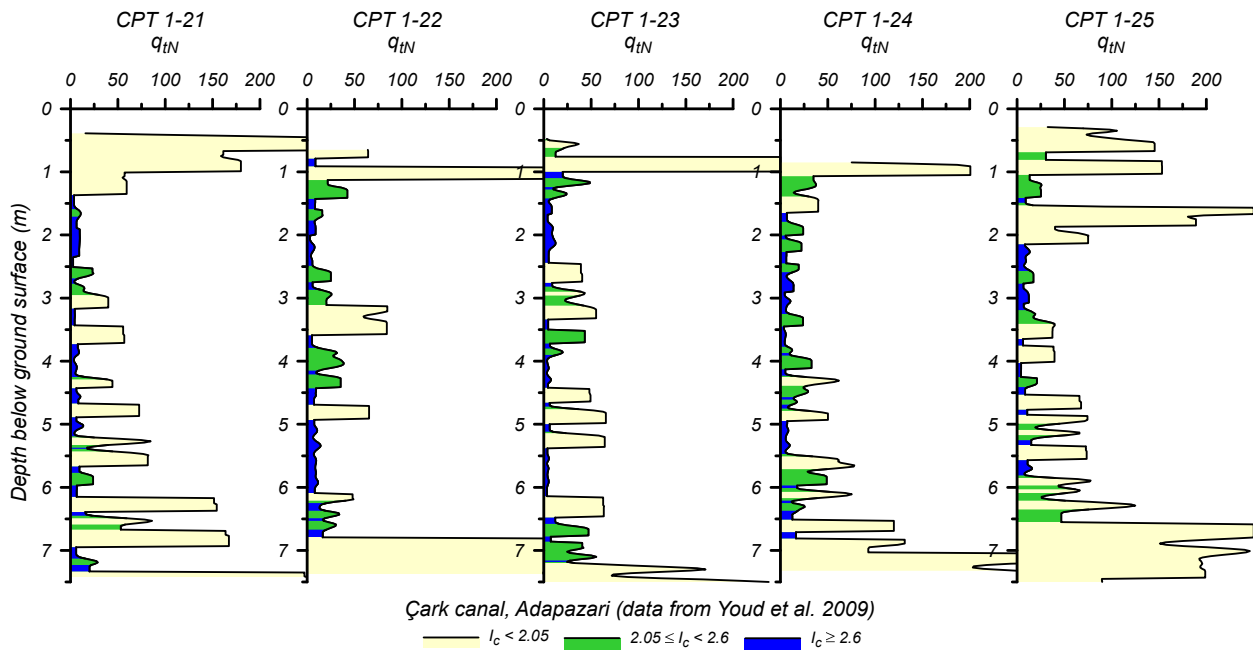
Figure 6. Cone penetration test profiles after application of the inverse filtering procedure using the baseline set of filter parameters from Boulanger and DeJong (2018)

6
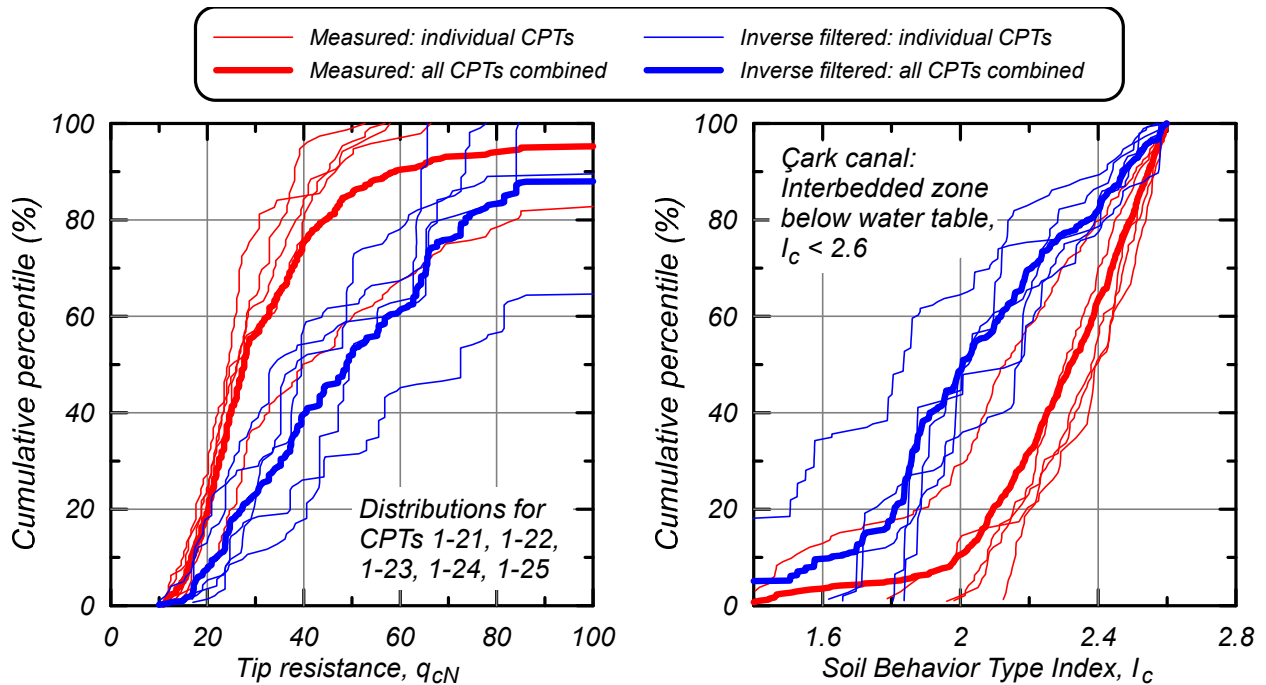
Figure 7. Cumulative distributions of tip resistance and I_c for the sand-like soils within the interbedded stratum beneath the water table for the measured CPT data (red lines) and inverse filtered data (blue lines)
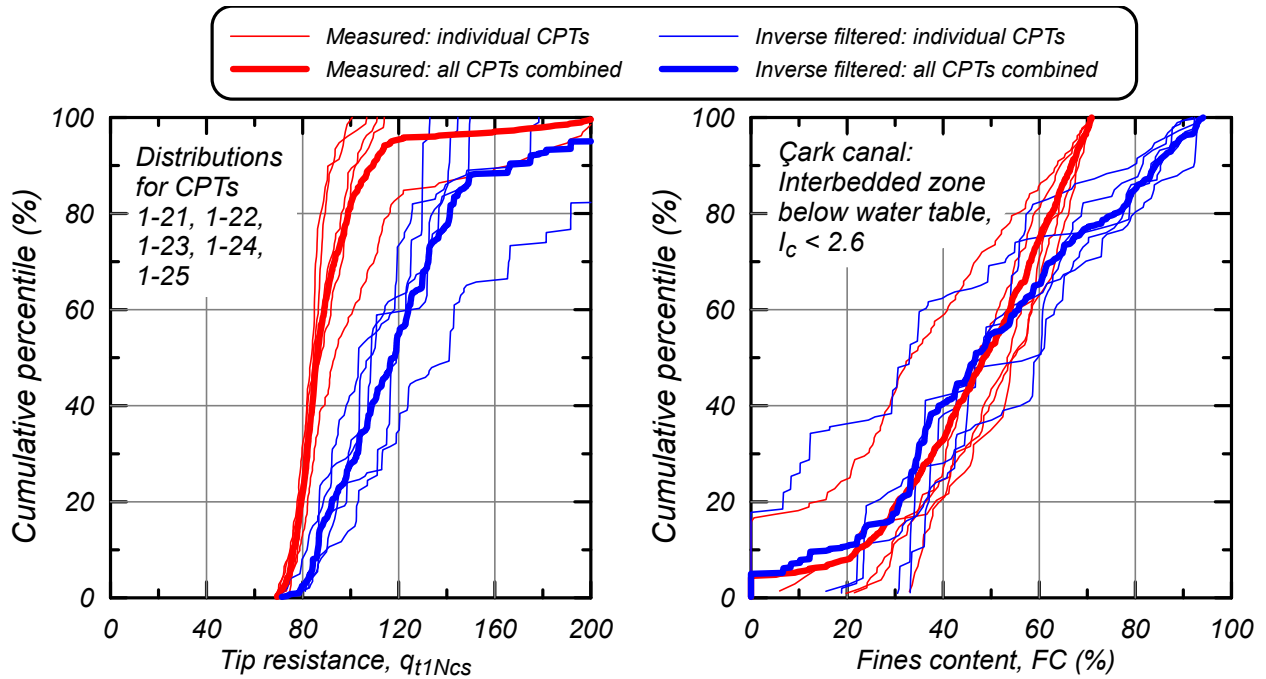
Figure 8. Cumulative distributions of equivalent clean sand, overburden-corrected tip resistance and fines content for the sand-like soils within the interbedded stratum beneath the water table for the measured CPT data (red lines) and inverse filtered data (blue lines)

7
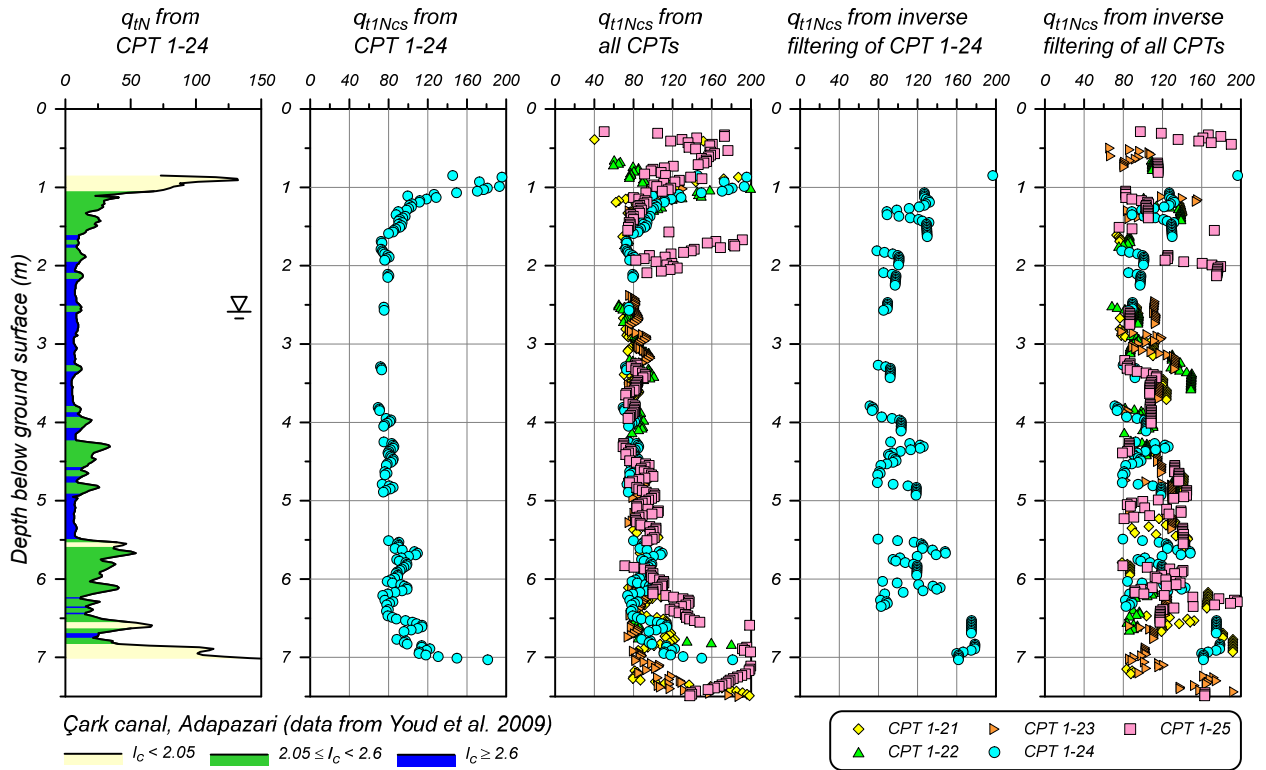
Figure 9. Equivalent clean sand, overburden corrected penetration resistances in the sand-like soils with and without the inverse filtering procedure of Boulanger and DeJong (2018)
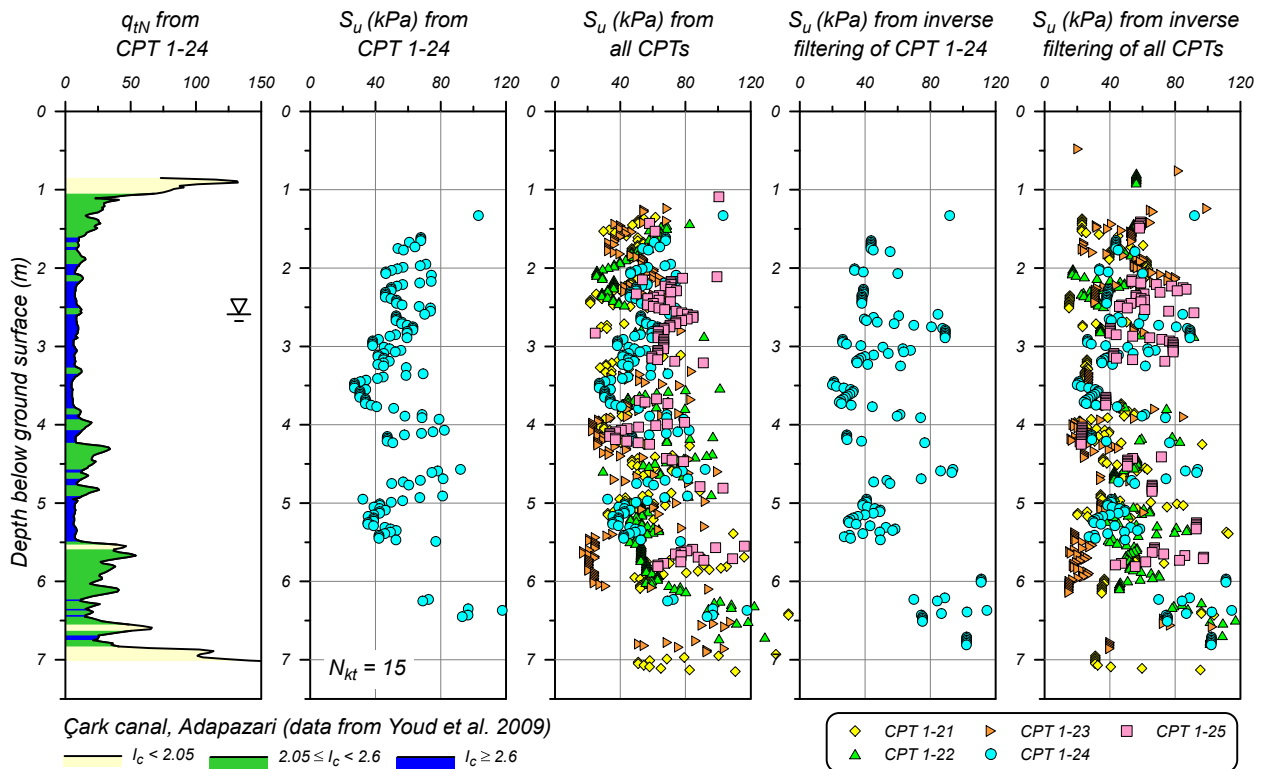
Figure 10. Undrained shear strengths in the clay-like soils with and without the inverse filtering procedure of Boulanger and DeJong (2018)
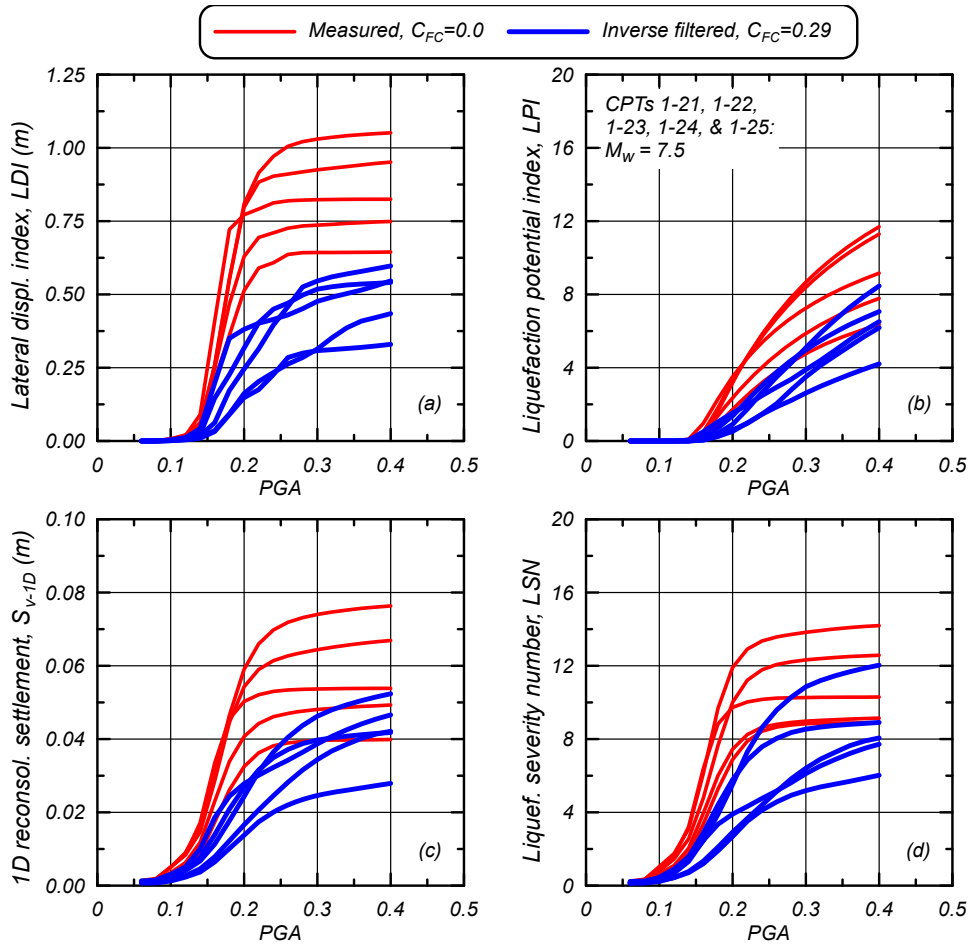
Figure 11. Liquefaction vulnerability indices versus peak ground acceleration for measured and inverse filtered CPT data with site-specific fines content calibrations: (a) LDI, (b) LPI, (c) $S_{v\text{-}1D}$, and (d) LSN. Note that the PGA at the site in the Kocaeli earthquake is estimated to be about 0.36 g.
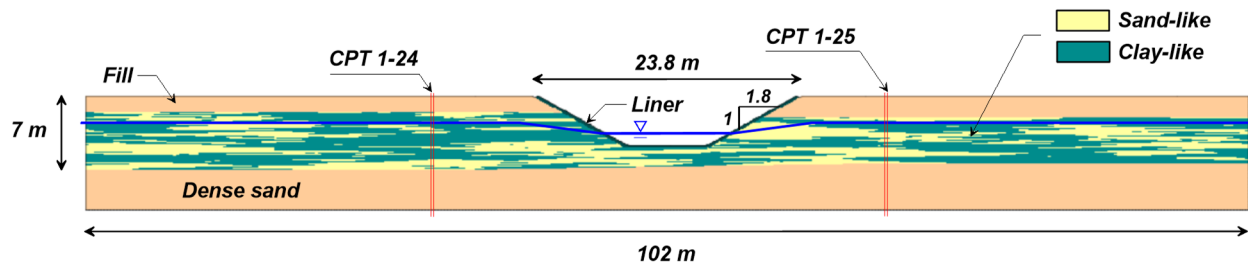
Figure 12. FLAC model with major zones and water table
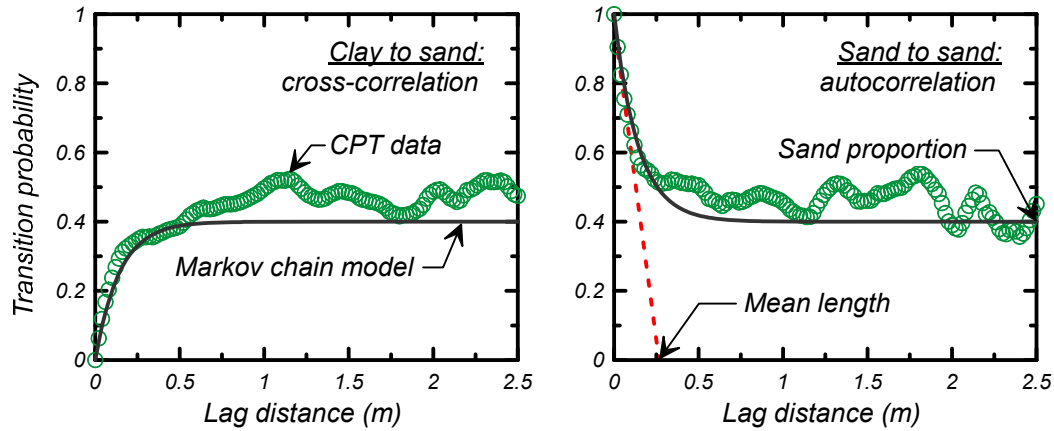
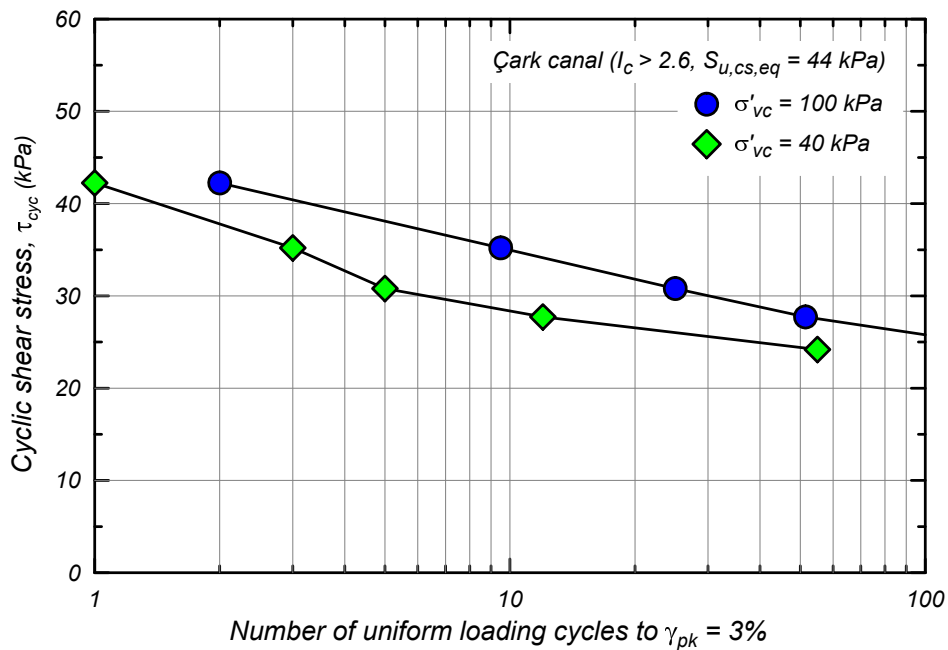Figure 13. Transition probability data and models for vertical direction based on the five CPT soundings (Munter et al. 2017)

Figure 14. Cyclic strength curves for the clay-like soils at two overburden stresses from single element simulations of undrained DSS loading with PM4Silt
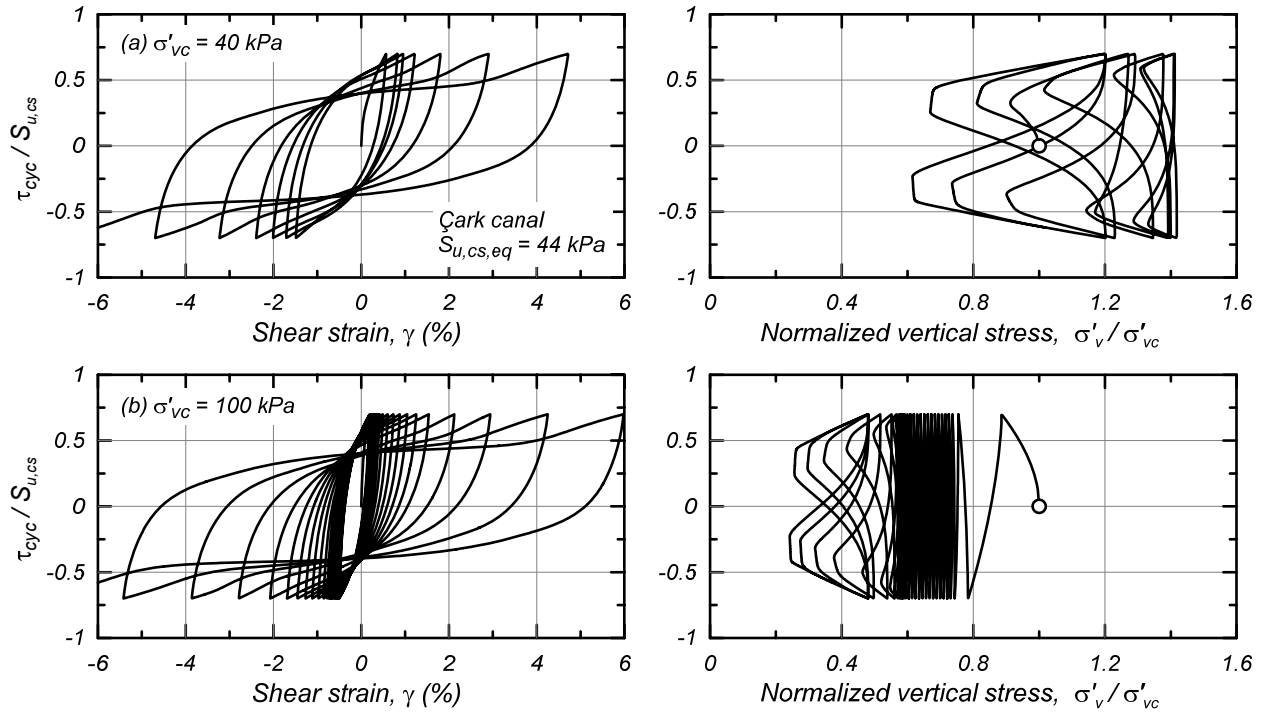
Figure 15. Cyclic stress-strain responses for the clay-like soils at two overburden stresses from single element simulations of undrained DSS loading with PM4Silt
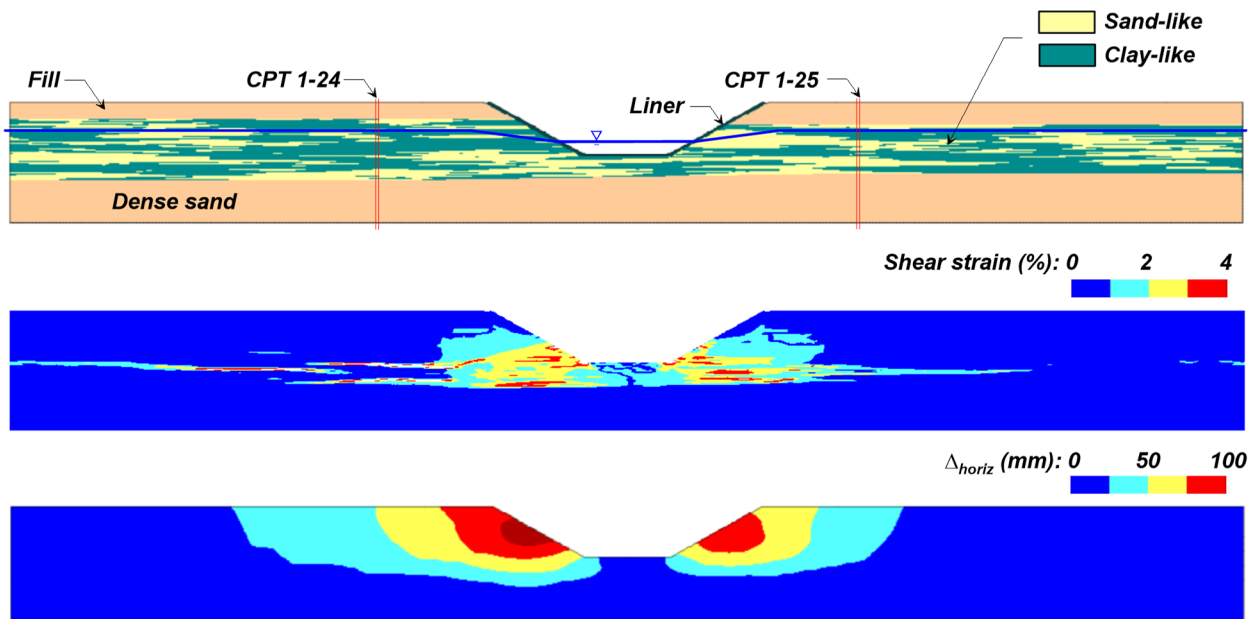

Figure 16. Stratigraphy, shear strains, and lateral displacements for a realization using $L_z = 0.26$ m, $L_x = 10$ m, and $q_{t1Ncs} = 115$ for the sand-like portions of the interbedded stratum
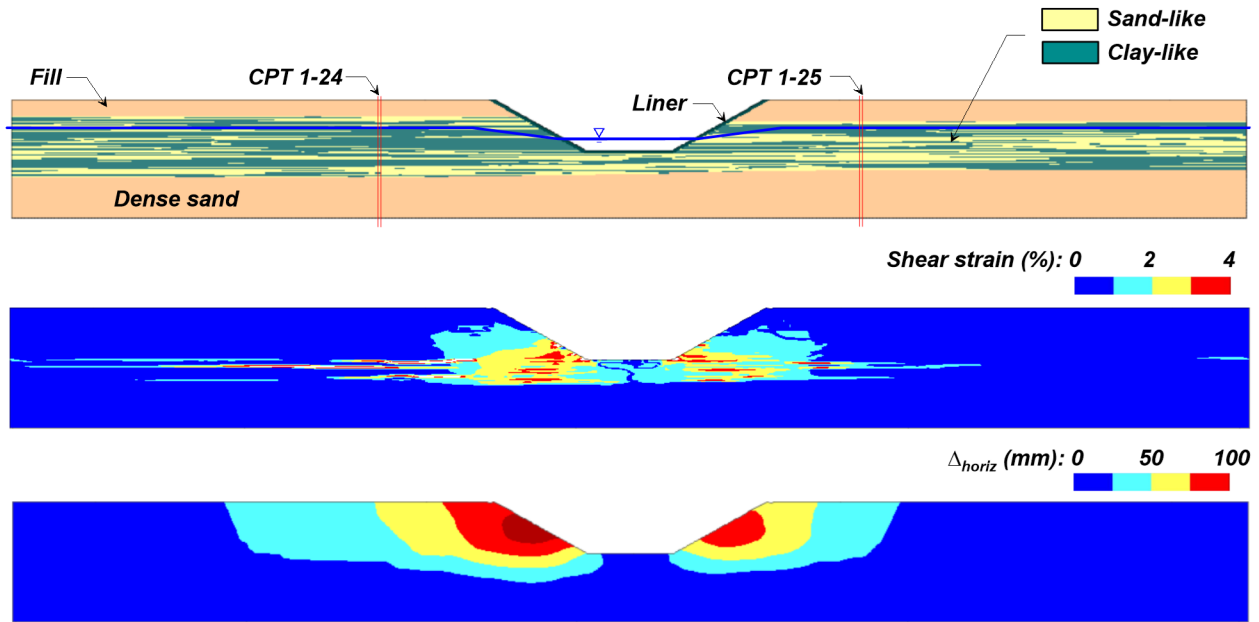
Figure 17. Stratigraphy, shear strains, and lateral displacements for a realization using $L_z = 0.26$ m, $L_x = 40$ m, and $q_{t1Ncs} = 115$ for the sand-like portions of the interbedded stratum
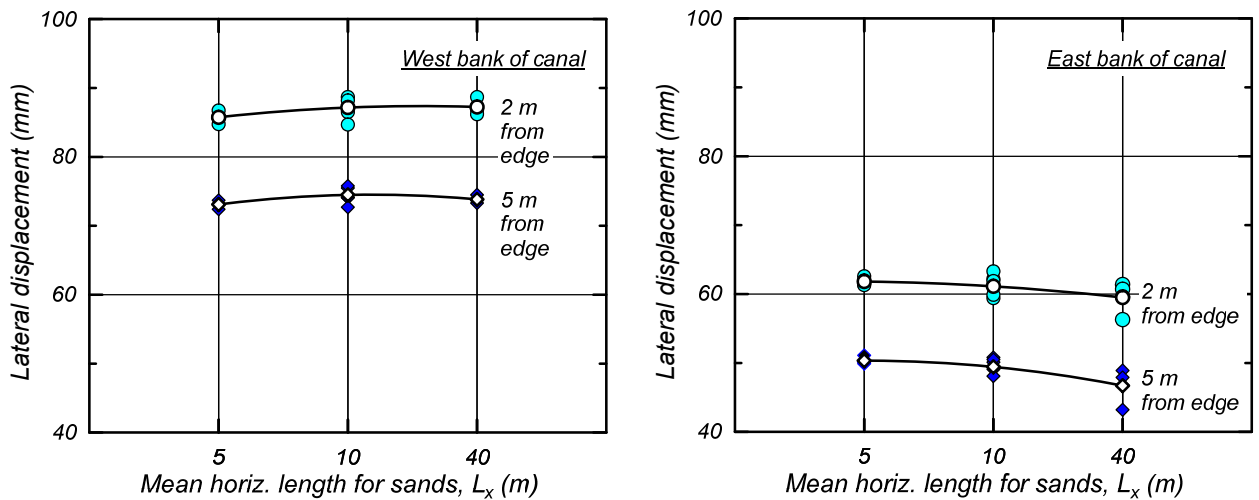

Figure 18. Lateral displacement toward canal on the west and east banks for points located 2 and 5 m from the edges of the canal using $q_{c1Ncs} = 115$ for the sand-like portions of the interbedded stratum